Magnetization of Gd diffused $YBa_2Cu_3O_{7-x}$ superconductor: Experiment and theory

Magnetization of Gd diffused $YBa_2Cu_3O_{7-x}$ superconductor: Experiment and theory

F. Inanir[a)], Ş. Yildiz[b)†], K. Ozturk[c)], and S. Celebi[c)]

[a)] *Department of Physics, Art and Science Faculty, Recep Tayyip Erdogan University, 53100, Rize, Turkey*
[b)] *Department of Metallurgical and Materials Engineering, Ahi Evran University, 40100, Kırsehir, Turkey*
[c)] *Department of Physics, Karadeniz Technical University, 61000, Trabzon, Turkey*

(Received 22 May 2012; revised manuscript received 18 January 2013)

The magnetization of Gd diffused $YBa_2Cu_3O_{7-x}$ is measured by a vibrating sample magnetometer (VSM) at selected temperatures (5, 25, 50, 77 K). The experimental results for the magnetization are analyzed in the critical state framework involving Kim–Anderson field dependence $J_c(H) = J_{c0}/(1+|H|/H_0)^n$ of critical current density and equilibrium magnetization M_{eq}. It is found that the inclusion of the equilibrium magnetization becomes more important at higher temperatures. At 77 K, the shape of the isothermal *M–H* hysteresis curve is governed by the equilibrium magnetization. Some superconducting parameters are determined by fitting the calculated curves to the experimental data.

Keywords: type-II superconductor, YBCO, surface effect, equilibrium magnetization, critical-state model

PACS: 74.81.Bd, 74.25.Ha, 74.25.Wx **DOI:** 10.1088/1674-1056/22/7/077402

1. Introduction

The critical state model has often been employed to study critical magnetic field, Meissner expulsion, trapped flux, hysteresis losses, and characteristic lengths from magnetization measurements. The investigations of equilibrium magnetization in the mixed state of high-T_c superconductors, which exhibit reversible behavior in an extremely wide range of magnetic fields, provide the valuable information about different parameters such as the lower critical field H_{c1}, upper critical field H_{c2}, and the thermodynamic critical field H_c.[1–3] These parameters can give straightforward information about the other superconducting parameters such as the superconducting coherence length and magnetic penetration depth.

Investigations on $RE Ba_2Cu_3O_{7-x}$ (*RE* is rare earth elements such as Nd, Sm, Eu, Gd) superconductors have shown that these materials each show higher T_c, higher J_c in the magnetic field, and larger irreversible field, than $YBa_2Cu_3O_{7-x}$ (YBCO).[4–6] Both Y and Ba sites in YBCO compound are substituted by the rare earth elements. The correlations of solution energies (of Lu, Ho, Gd, Eu, and La) with ion size are observed for trivalent rare earth ion substitution of barium. Substitutions of large rare earth ions are energetically more desirable at Ba site.[7] Koshizuka *et al.*[8] have shown that *RE*/Ba substitution into bulk $RE Ba_2Cu_3O_{7-x}$ (*RE*BCO) superconductors was highly attractive since the substitutions could work as pinning centres in the magnetic field. Generally, other rare earth elements such as *RE* = Y, Nd, Sm, Er, Eu, etc. with the identical crystal structure can replace the Gd sites. However, the difference between the ionic radii of *R* occurs differently in the electronic state on the CuO_2 plane and affects the transition temperature T_c.[9] Commonly, the features of grain boundaries in YBCO are unlike those of bulk materials. This discrepancy leads to weak intergrain links and limits critical currents in a superconductor.[10] It was reported[11,12] that the doping of YBCO with Gd and Ca resulted in the substantial enhancement of the grain boundary critical current density J_c. The magnetic property of superconductor is also interesting because a secondary peak, the so-called fish-tail peak of magnetization hysteresis loop on Gd-doped YBCO sample, has been identified.[13–15] However, much work [16,17] on Y substituted by rare-earth elements (denoted as $Y_{1-x}RE_xBCO$) has been devoted to the relationship between the magnetic ordering and superconductivity.

In the present paper, the magnetization measurements each as a function of applied field up to 3 T on Gd diffused YBCO are carried out at different temperatures. The equilibrium property of this specimen is extracted from *M–H* loops. Equilibrium (reversible) magnetization M_{eq} curves versus applied field H_a are obtained employing Kim–Anderson critical state model with taking the equilibrium surface current into account. Some superconducting parameters are obtained by comparing the calculated results based on the critical state model with the experimental data measured at four selected temperatures.

2. Experiment

Superconducting YBCO samples were prepared by the solid state reaction method from high-purity starting powders

†Corresponding author. E-mail: sukruyldz@gmail.com

Y_2O_3, $BaCO_3$, and CuO. The powders were thoroughly mixed in the desired proportions and then heated in air for 24 h at 900 °C in a square muffle furnace with heating and cooling rate of 5 °C·min^{-1} and 1 °C·min^{-1}, respectively. After cooling to room temperature, the powder was ground and pressed under 400 MPa into pellets with 13 mm in diameter. Then, these pellets were sintered at 930 °C in air for 24 h, followed by oxygenation at 500 °C.

The Gd diffusion in YBCO pellets was carried out using an ultra-high vacuum electron-beam deposition system to obtain Gd layers with approximately 4 μm in thickness on one side surface of the sample. The diffusion annealings of samples, which will hereafter be denoted as Gd900, with the deposited Gd layer were executed in air, respectively, at temperatures 900, 850, 800, 700, and 600 °C for 12 h.

The magnetization properties were measured using a vibrating sample magnetometer (VSM) composed of the Quantum Design PPMS system, respectively, at constant temperatures such as 5, 25, 50, and 77 K with the magnetic field along the direction perpendicular to the diffusion-doped surface. All the measurements were performed at a sweep rate of 5 mT·s^{-1} upon zero field cooling (ZFC) process. Before each measurement at different temperature, we heated the sample above the transition temperature T_c after completing the isothermal magnetization curve at a selected temperature to remove the trapped magnetic flux from the sample. All samples were rectangular and their typical dimensions were 0.5 mm × 3.3 mm × 2.8 mm for magnetization studies.

3. Theoretical framework of our analysis

We consider a superconducting slab specimen of dimensions larger compared with the penetration depth of magnetic field λ and a magnetic field is applied parallel to its surface. Magnetization M for an idealized slab is calculated by

$$\langle M\rangle = \langle H_i\rangle - H_a = \frac{1}{W}\int_0^W (H(x)-H_a)\,\mathrm{d}x, \tag{1}$$

where W is the thickness of the slab, $H(x)$ is the local flux density permeating the slab along the applied field H_a and the surfaces of the slab are situated at $-W \le x \le W$. To calculate $B(x) = \mu_0 H(x)$ the critical state framework is employed. The magnetic flux profile $H(x)$ inside the superconducting slab sample obeys the Maxwell's equation

$$\frac{\partial H}{\partial x} = \pm J_c, \tag{2}$$

where the signs "+" or "−" is determined by the slope of the flux density in the specimen. The critical current density $J_c(H)$ is deduced to be of Kim type,[18,19] which gives the best description of many observations of hysteretic M–H curves in high-T_c superconductors and a remarkably good fitting to our experimental data is obtained, thus

$$J_c(H,T) = \frac{J_{c0}(T)}{\left(1+\frac{|H|}{H_0(T)}\right)^n}, \tag{3}$$

where H_0 and n are phenomenological parameters and J_{c0} is the critical current density at zero magnetic field. Here, the boundary condition for Eq. (2) is $H(x=0) = H(x=W) = H_a$. From the symmetry it is sufficient to consider only the half-part of the slab. The solutions to Eqs. (2) and (3) for the given boundary condition, respectively, are

$$H_{\pm}(x) = -H_0 + H_0\left[(1+|H_s|/H_0)^{n+1} \mp p(1-x/W)\right]^{1/(n+1)} \tag{4}$$

and

$$H_{\pm}(x) = -H_0 + H_0\left[2-(1-|H_s|/H_0)^{n+1} \mp p(1-x/W)\right]^{1/(n+1)}, \tag{5}$$

where

$$p = \frac{(n+1)J_{c0}W}{H_0}, \tag{6}$$

and the full-penetration field H_p is

$$H_p = H_0(1-p^{1/(n+1)}). \tag{7}$$

Here H_s describes the magnetic flux density $H(x)$ at the surface $x = W - \lambda$. Equation (4) is used when H_s is ascending (descending) in the $+z$ direction and equation (5) determines the flux profile in the inner space, $0 \le x \le x_0$; when H_s after descending from a large positive value increases beyond H_{c1} in the negative direction. x_0 is the plane where $H_{\pm}(x = x_0) = 0$. There are two further solutions of Eqs. (2) and (3) which can be obtained from Eqs. (4) and (5) by replacing $H(x)$ by $-H(x)$ and H_s by $-H_s$, respectively.

The role of lower critical filed H_{c1} in magnetizing the type II superconductor has been investigated.[20–23] Celebi *et al.*[21–23] reported that the magnetization curve is somewhat complicated due to non-zero value of H_{c1}, while the effective field at the sample surface may be described by

$$H_s = \frac{M_{eq}}{\mu_0} = H_a - I_M, \tag{8}$$

where I_M describes the diamagnetic Meissner surface current flowing along the direction perpendicular to H_a, and M_{eq} denotes the equilibrium (reversible) Abrikosov diamagnetism. Over the range $0 \le H_a \le H_{c1}$, $I_M = H_a$, and $H_s = 0$ for all previous histories of applied field, hence for all configurations of $H(x)$. For $H_{c1} < H_a < H_{c2}$, we use the simple approximation,

$$I_M = \frac{H_{c1}^{k+1}}{H_a^k}, \tag{9}$$

where k is Meissner exponent and regarded as a temperature-dependent parameter. The full cycle of M versus H_a can be obtained employing the method presented by Chen and Goldfarb.[24]

The magnetization curve obtained using the original critical state approximation is symmetric about $M = 0$, with mag-

nitude $M_s = (f/2)J_{c0}W$. Here f defines the geometric factor (1/2 for a slab, 1/3 for a cylinder). If the effective $M_{eq}(H)$ is involved, the $B(x)$ field profiles retain their shapes but are shifted to a value given in Eq. (8) on the surface.[25] Expressing the magnetization in the increasing and decreasing form by $M_\uparrow(H)$ and $M_\downarrow(H)$ respectively, we have $M_\uparrow(H) = M_{eq}(H) - (f/2)J_cW$ and $M_\downarrow(H) = M_{eq}(H) + (f/2)J_cW$, and the hysteresis curves are symmetric about $M_{eq}(H)$. Therefore, $M_{eq}(H)$ and $J_c(H)$ can be written as

$$M_{eq}(H) = \frac{1}{2}(M_\uparrow(H) + M_\downarrow(H)) \tag{10}$$

and

$$J_c(H) = \frac{1}{2fW}(M_\downarrow(H) - M_\uparrow(H)). \tag{11}$$

Equation (11) has been used extensively to obtain $J_c(B)$ from the magnetization hysteresis $\Delta M(H) = (M_\downarrow(H) - M_\uparrow(H))$ at $H_a = B_a/\mu_0$.

4. Result and discussion

In Fig. 1 (empty symbols), we display magnetization curves of the same sample measured at several temperatures. Under a constant applied external field, magnetization decreases as temperature increases, whereas the curves vary gradually not only in magnitude but also in general shape. The entire magnetization loop measured at 10 K exhibits a very small downward shift (to diamagnetic quadrant) but neither reversible nor semi-reversible behavior. While the descending branch of *M*–*H* hysteresis at 25 K shifts towards the diamagnetic quadrant, the loci of *M*–*H* curves at 50 K and 77 K travel entirely with diamagnetic quadrants of magnetization. This behavior can be explained as the fact that the diamagnetic moment (equilibrium magnetization) produced by the shielding Meissner current I_M circulating along the surface of individual grains contributes to the irreversible magnetization in a direction opposite to the paramagnetic moment generated by the flux retaining currents circulating inside the volume of each grain. We note that the magnetization curve at 77 K exhibits a nearly reversible behavior and also the diamagnetic moment descends very rapidly with H_a decreasing in the range $0 < H_a < H_{c1}$, thereby allowing the paramagnetic moment produced by the flux retaining-induced current to occur manifestly.

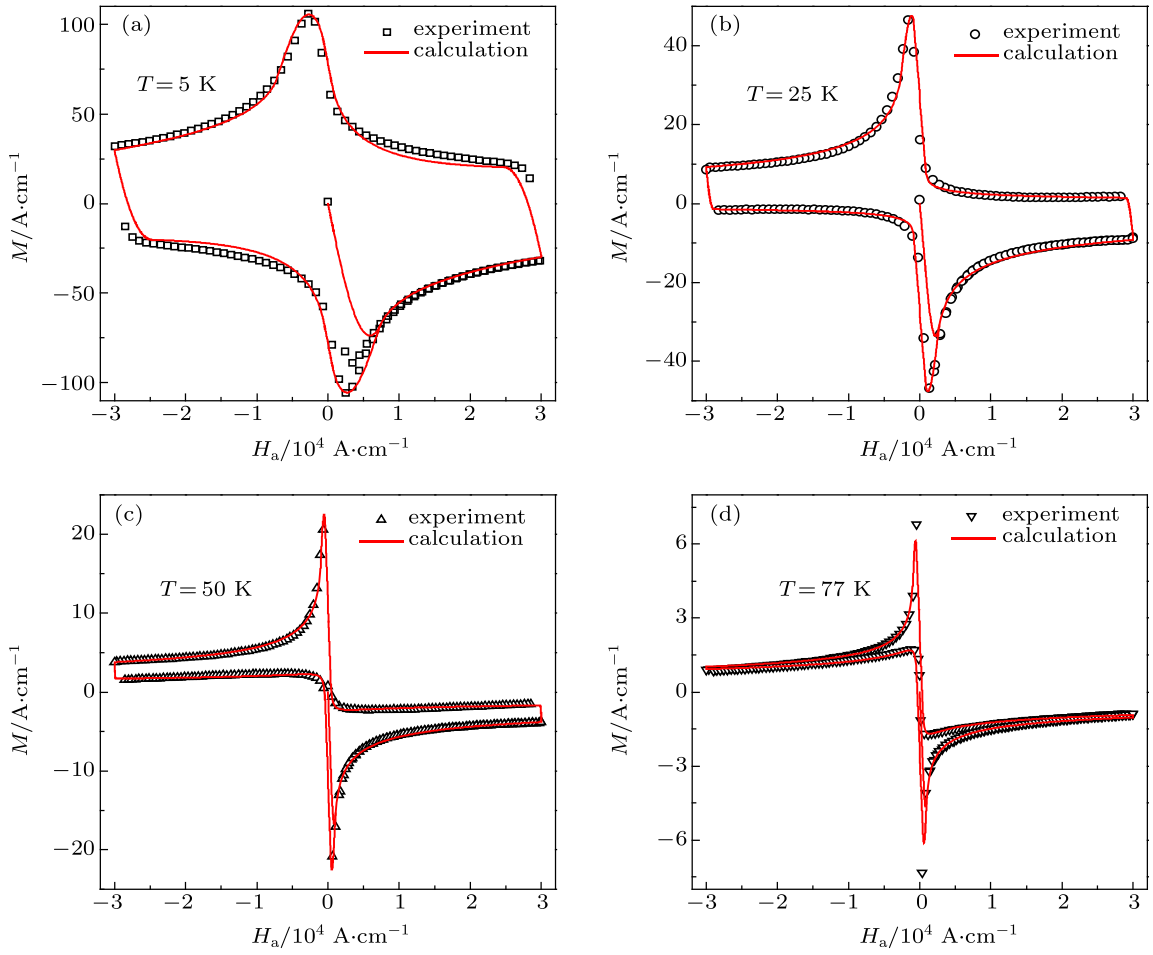

Fig. 1. (color online) Experimental magnetization loops (empty symbols) and corresponding theoretically-predicted curves (solid lines) of the investigated Gd-diffused YBCO slabs at (a) 5 K, (b) 25 K, (c) 50 K, and (d) 77 K. Theoretical values are calculated using Eqs. (1)–(9), whereas parameters employed in calculations are given in Table 1.

The experimental data in Fig. 1 can successfully be fitted to Eqs. (1)–(9) (solid lines), where the generalized Kim's model can reproduce the observed magnetization curves excellently over the whole experimental field range and at all temperatures of interest. We have ignored the demagnetization effect in the calculation. In our work we have used these formulas and a general computer program in which a variety of simple expressions for $J_c(B)$ are adopted. The fitting parameters are also given in Table 1. In this calculation, the controllable parameters are H_0, n, H_p, k, and H_{c1}. All parameters are considered as being temperature-dependent. The lower critical field H_{c1} is adopted to produce the equilibrium magnetization. We have determined the full penetration field H_p from the measured hysteresis curve which is defined as the external field required for first penetration of flux lines to the central axis of the sample. This value also accords with the coalescence point of the initial magnetization curve and the ascending parts of the fully magnetized curve at the same external field. The exponent n for critical current and k for Meissner current are assessed to be the best fitting to the experimental curve. We estimate that these parameters should also be temperature-dependent. The surface barrier current is ignored since measurements do not reveal the influence of any significant surface barrier current such as a straight line in the traversal M–H loops between the upper and the lower branches.[26] Geometric barrier effects are also ignored[26–29] since the demagnetization factors for all our samples are all very small and these are important only at low field.[30] We do not think that the coexistence of superconductivity and paramagnetism is due to paramagnetic Gd ions[17] since we do not observe the sign changing in diamagnetic moment (negative to positive) at a certain value of external field as the magnetic field ascends after zero magnetic field. Although there are many factors affecting the magnetic behavior of granular superconductor specimen such as the size, shape, and orientation of the grain, anisotropy of current flow, flux pinning property of grain, matrix and coupling property of grain, etc., the proposed model is sufficient to reproduce the experimental data extremely well and also to determine some important superconducting parameters, such as those in Table 1.

Table 1. Fitting parameters describing the field-dependent critical current density according to the Kim–Anderson model: $J_c(H) = J_{c0}/(1+|H|/H_0)^n$ including equilibrium magnetization M_{eq} defined by Eqs. (8) and (9).

T/K	n	H_{c1}/A·cm^{-1}	H_0/A·cm^{-1}	H_p/A·cm^{-1}	k
5	0.43	789.4	300.2	4838.7	0.0008
25	0.45	90.9	181.5	2721.6	0.45
50	0.5	30.3	420.1	1210.2	0.81
77	0.86	5.2	159.1	978.0	3

Theoretical contributions of equilibrium magnetization to the critical state magnetization at 5 K and 77 K can be visually assessed by comparing each pair of adjacent curves illustrated in Figs. 2(a) and 2(b). We note that the presence of the equilibrium magnetization can considerably enhance the scale of the magnetization curve and also changes its shape. The model used for the equilibrium magnetization is plotted in Fig. 3 along with the experimental values obtained from Eq. (10). The equilibrium (reversible) magnetization curve M_{eq} (H) has an 180°-rotation symmetry containing a linear interval between H_{c1} and $-H_{c1}$ and peaks around them. One can infer that there is strong diamagnetism around lower critical field. The observed $M_{eq}(H)$ maxima around H_{c1} imply that there can be an additional loss mechanism which has a large function around $\pm H_{c1}$. The loss can be caused by depinning of the vortices pinned to the sample surface, since surface pinning makes $H > H_{c1}$ at the flux entrance and $H < H_{c1}$ at the flux exit held. Thus, ac losses could occur even without defects serving as internal pinning centers.

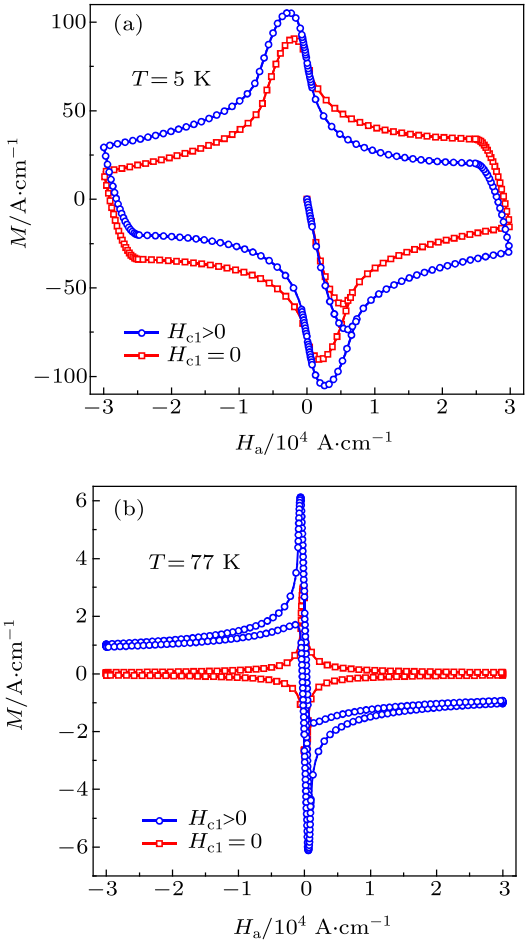

Fig. 2. (color online) The calculated curves with empty circles in panels (a) and (b) are the same as those in Figs. 1(a) and 1(d), respectively. The empty rectangular curves in panels (a) and (b) represent the calculations with the same inputs as their partners but with $H_{c1} = 0$, hence with no equilibrium contribution to the magnetization.

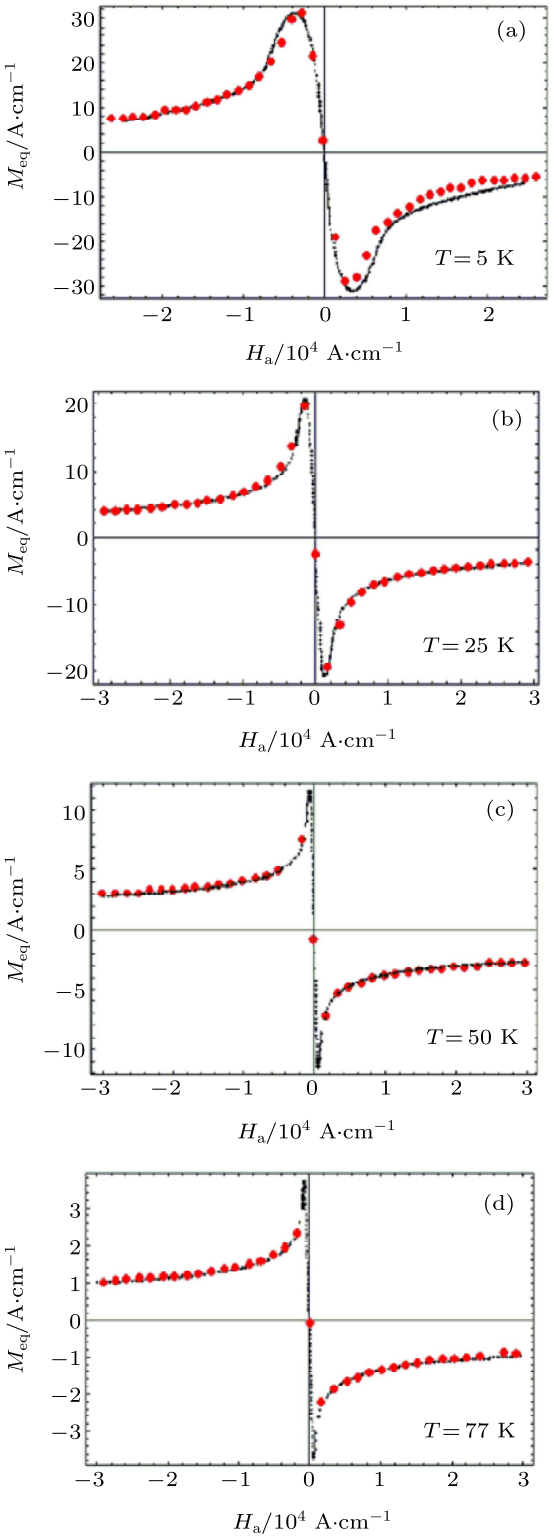

Fig. 3. Experimental and theoretical equilibrium magnetization curves each as a function of applied field for different temperatures. Parameters are the same as those in Fig. 1. To obtain the equilibrium magnetization curve from *M–H* loops, equation (10) is used.

5. Conclusions

The values of DC magnetization in Gd diffused YBCO prepared by a solid state reaction method are measured at various temperatures using vibrating sample magnetometer in magnetic fields up to 3 T. In order to clarify equilibrium magnetization influence on *M–H* curve, which plays an important role in the mixed state of high-T_c superconductors, the experimental magnetization hysteresis loops are fitted employing critical state model. The fitted curves in the Kim–Anderson model, $J_c(H) = J_{c0}/(1+|H|/H_0)^n$, in the case of $H_{c1} \neq 0$ and thus $M_{eq}(H) \neq 0$ are in good consistency with the experimental data, so that certain material parameters could be successfully obtained. It is concluded that the Gd diffusion causes a mixed state property ruled by Meissner surface current whose efficiency decreases with the decrease of the induced magnetic field inside the superconductor. As shown from the fitting data in Table 1, the Meissner exponent, k, increases with temperature increasing. This reduces the effect of the Meissner surface current.

References

[1] Hao Z and Clem J R 1991 *Phys. Rev. Lett.* **67** 2371
[2] Hao Z and Clem J R, McElfresh M W, Civale L, Malezemoff A P and Holtzberg F 1991 *Phys. Rev. B* **43** 2844
[3] Landau I L and Ott H R 2004 *Physica C* **411** 83
[4] Murakami M, Sakai N, Higuchi T and Yoo S I 1996 *Supercond. Sci. Technol.* **9** 1015
[5] Miyachi K, Sudoh K, Ichino Y, Yoshida Y and Takai Y 2003 *Physica C* **392–396** 1261
[6] Nishida A, Teshima S and Taka C 2002 *Physica C* **378–381** 349
[7] Islam M S and Baetzold R C 1989 *Phys. Rev. B* **40** 10926
[8] Koshizuka N, Pradhan A K, Shibata S, Feng Y, Machi T and Nakano K 2001 *Physica C* **364–365** 320
[9] Veal B W, Paulikas A P, Downey J W, Claus H, Vandervoort K, Tomlins G, Shi H, Jensen M and Mors L 1989 *Physica C* **162–164** 97
[10] Hilgenkamp H, Scheider C W, Schulz R R, Goetz B, Schmehl A, Bielefeldt H and Mannhart J 1999 *Physica C* **326–327** 7
[11] Nishida A, Teshima S, Taka C and Shigeta I 2003 *Physica C* **388–389** 419
[12] Berenov A V, Foltyn S R, Schneider C W, Warburton P A and MacManus-Driscoll J L 2003 *Solids State Ionics* **164** 149
[13] Yong F, Lian Z, Wen J G, Koshizuka N, Sulpica A, Tholence J L, Vallier J C and Monceau P 1998 *Physica C* **297** 75
[14] Muralidhar M, Koblischka M R and Murakami M 1999 *Physica C* **313** 232
[15] Johansen T H, Koblischka M R, Bratsberg H and Hetland P O 1997 *Phys. Rev. B* **56** 11273
[16] Furayama M, Iguchi I and Muto U 1990 *Physica B* **165–166** 1191
[17] Qin M J, Ji H L, Jin X, Yao X X, Rong X S, Ni Y M, Xiao L and Fu X K 1994 *Phys. Rev. B* **50** 4086
[18] Kim Y B, Hempstead C F and Strnad A R 1962 *Phys. Rev. Lett.* **9** 306
[19] Kim Y B, Hempstead C F and Strnad A R 1963 *Phys. Rev.* **131** 2486
[20] Chen D X and Sanchez A 1992 *Phys. Rev. B* **45** 10793
[21] Çelebi S, Inanir F and LeBlanc M A R 2007 *J. Appl. Phys.* **101** 13906
[22] Celebi S, Ozturk A and Cevik U 1999 *J. Alloys Compd.* **288** 249
[23] Celebi S, Ozturk A, Yanmaz E and Kobya A I 2000 *J. Alloys Compd.* **298** 285
[24] Chen D X and Goldfarb R B 1989 *J. Appl. Phys.* **66** 2489
[25] de Gennes P G 1966 *Superconductivity of Metals and Alloys* (New York: Benjamin) p. 83
[26] LeBlanc M A R, Fillon G, Timms W E, Zahradnitsky A and Cave J R 1981 *Cryogenics* **21** 491
[27] Idenbom M V, Kronmüller H, Li T W, Kes P H and Menovsky A A 1994 *Physica C* **222** 203
[28] Schuster T H, Idenbom M V, Kuhn H, Brandt E H and Konczykowski M 1994 *Phys. Rev. Lett.* **73** 1424
[29] Zeldow E, Larkin A I, Geshkenbein V B, Konczykowski M, Majer D, Khaykovich B, Vinokur V M and Shtrikman H 1994 *Phys. Rev. Lett.* **73** 1428
[30] Burlachkov L, Yeshurun Y, Konczykowski M and Holtzberg H 1992 *Phys. Rev. B* **45** 8193